United States
Department of
Agriculture

Forest Service

Forest Pest
Management

Davis, CA

# Effect of Upwind-Downwind Aircraft Vortex Decay on Ground Deposition

FPM 95-13
May 1995

Pesticides used improperly can be injurious to human beings, animals, and plants. Follow the directions and heed all precautions on labels. Store pesticides in original containers under lock and key—out of the reach of children and animals—and away from food and feed.

Apply pesticides so that they do not endanger humans, livestock, crops, beneficial insects, fish, and wildlife. Do not apply pesticides where there is danger of drift when honey bees or other pollinating insects are visiting plants, or in ways that may contaminate water or leave illegal residues.

Avoid prolonged inhalation of pesticide sprays or dusts; wear protective clothing and equipment, if specified on the label.

If your hands become contaminated with a pesticide, do not eat or drink until you have washed. In case a pesticide is swallowed or gets in the eyes, follow the first aid treatment given on the label, and get prompt medical attention. If a pesticide is spilled on your skin or clothing, remove clothing immediately and wash skin thoroughly.

---

NOTE: Some States have restrictions on the use of certain pesticides. Check your State and local regulations. Also, because registrations of pesticides are under constant review by the U.S Environmental Protection Agency, consult your local forest pathologist, county agriculture agent, or State extension specialist to be sure the intended use is still registered.

FPM 95-13
(C.D.I. Technical Note 95-02)
May 1995

# Effect of Upwind-Downwind Aircraft Vortex Decay on Ground Deposition

Prepared by:

Milton E. Teske
Alina Z. MacNichol

Continuum Dynamics, Inc.
P.O. Box 3073
Princeton, NJ 08543

Contract No. 53-0343-4-00009

Prepared for:

USDA Forest Service
Forest Health Technology
Enterprise Team
Davis Service Center
2121C Second Street
Davis, CA 95616
(916)757-8341
FAX (916)757-8383

John W. Barry
Project Officer

# SUMMARY

Tower anemometer flyby data, collected principally from the Program WIND (Winds In Nonuniform Domains) field trials, and used previously to deduce the decay rate of the strength of aircraft vortex pairs near the ground, are re-examined here to extract the effect of crosswind shear on the decay of the upwind vortex strength relative to the downwind vortex strength. This analysis involves revisiting the previous algorithm, generalizing it to permit different upwind and downwind vortex strengths, then generating results obtained with crosswind shear affecting the two vortices (lessening the decay of the upwind vortex, while enhancing the decay of the downwind vortex). The correlated results are then used to initiate a series of computer simulations, using the FSCBG (Forest Service Cramber-Barry-Grim) aerial application model, to compare ground deposition due to nozzles on the upwind spray boom with ground deposition due to nozzles on the downwind spray boom. An analytical model of vortices in crosswind, and available deposition data from two field studies conducted recently in New Mexico, are used to demonstrate the apparent influence of crosswind shear on deposition.

The simple vortex model present in the near-wake in FSCBG is shown to predict the same trends as the upwind-downwind data from the field studies (with spray material released from the downwind nozzles more prone to drift than spray material released from the upwind nozzles). However, atomization from the downwind nozzles appears to include more smaller drops than atomization from the upwind nozzles, which if true would distort the conclusions suggested by the New Mexico field studies. If the field studies were repeated, attention to nozzle atomization and modification of the study protocol to clarify any ambiguous areas should be high priorities. Such results would be eagerly awaited, as the upwind-downwind effect may then find quantification and enable us the improve our predictive model as well. An enhancement to the near-wake model in FSCBG may then include more detailed effects of crosswind, atmospheric turbulence and stability, and the ground than the present simpler approach provides. The field data would be used to validate an extended near-wake model in FSCBG, and bring closure to this problem in a timely manner.

# TABLE OF CONTENTS

# 1. INTRODUCTION

A series of aircraft flybys over tower grids instrumented with propeller anemometers was performed between 1985 and 1990. The first three sets of data were developed as a part of Program WIND (Winds In Nonuniform Domains) (Barry 1989); the last two sets were developed for the U. S. Army (Teske, Kaufman and Curbishley 1988 and 1990). The first three data sets took place from May through July 1985 at a cleared and a forested site (Foresthill Seed Orchard, CA) and an almond orchard (Hennigan Almond Orchard north of Chico, CA), and from late April to early May 1986 at a cleared sloping site in the Sierra Nevada foothills near Red Bluff, CA. The U. S. Army data sets took place in October 1988 and October 1990 at Dugway Proving Ground, UT. In all cases anemometer tower grids recorded the ambient vertical velocity time histories as various aircraft flew over the grid perpendicular to the tower line. These digitized velocity traces produced an aircraft wake signature that was then used to infer the strength and lateral and vertical motion of the aircraft vortex pairs generating the traces. A first report (Teske 1988) summarized the data collection from Program WIND (found in Williamson, Teske and Geyer 1985 and Teske 1986) and the algorithm developed to recover the vortex strength decay effects. Additional reports (Teske, Kaufman and Curbishley 1988 and 1990) detailed the collection and reduction of data from high-speed fighter aircraft at Dugway Proving Ground, and its correlation with the slower-speed aircraft of the Program WIND study.

From these results came the conclusion that ambient atmospheric turbulence worked to decay aircraft vortex strength in ground effect at a rate of 0.56 m/sec (Bilanin et al. 1989a and Teske, Bilanin and Barry 1993). This effect was incorporated into the near-wake model AGDISP (Bilanin et al. 1989b) of FSCBG, the Forest Service Cramer-Barry-Grim aerial spray model (Teske et al. 1993).

Recently, there has been renewed interest, both in the United States and Canada, on the effect of crosswind on the deposition pattern beneath agricultural aircraft. In a field study including nine field trials, McCooeye et al. (1993) found that ground deposition of mass from the upwind nozzles was on average 1.5 times that from the downwind nozzles out to 200 m. Since this result implies less drift of mass from the upwind side of the aircraft, it may also suggest a boom on/off strategy close to buffer zones or near sensitive areas. The authors implied that their results "clearly demonstrated the advantages of spraying from the upwind wing, both in terms of deposit of the small droplets and hence the reduction of off-target drift," even though number densities were not collected in the field study. In addition, some questions have surfaced regarding apparent differences in atomization from the upwind and downwind nozzles (Young 1993 and Mickle 1993). Fortunately, McCooeye et al. (1993) does contain enough information to conduct a series of preliminary FSCBG near-wake predictions and compare them to the trends suggested.

In a second field study Huddleston et al. (1994) suggested that the right boom makes a greater contribution to drift than the left boom, irrespective of crosswind direction. This surprising result is apparently a misinterpretation of their data, which actually demonstrates that drift was greater from the downwind nozzles in 12 of 18 trials, two trials gave essentially the same drift, and four trials showed more drift from the upwind nozzles. Unfortunately, very few details are available in the Huddleston et al. (1994) paper, and predictions of their specific results (which are in fact consistent with the McCooeye et al. 1993 results) cannot be attempted.

Thus, it would seem important to first re-examine the wealth of available tower data from Program WIND to see whether we can relax our algorithm assumptions and extract the upwind-downwind vortex strength effects in crosswind, then make near-wake FSCBG predictions more consistent with the McCooeye et al. (1993) field study. This investigation, and the results we find, form the subject of this report.

In the next section we review the tower data sets available to us, follow this data summary with the modified algorithm and its results, add the results from a previous numerical study on vortices in crosswind, then examine FSCBG simulations to determine the effect of upwind-downwind vortices on ground deposition.

# 2. TEST SUMMARY

Tables 1 through 4 summarize the digitized tower data recorded at Foresthill, Chico, Red Bluff and Dugway. The test procedure at these sites is reviewed in this section of the report.

## Test Aircraft

The aircraft used in the flybys included a Bell 206B helicopter, Cessna Ag Husky fixed wing, Hiller 12E helicopter, Schweizer Ag Cat biplane, C-130E four-engine fixed wing, and F-4, F-15 and F-16 high speed fighter aircraft. The intent of the combined series of data was to span the anticipated aircraft flight speeds for both slow-moving agricultural aircraft and higher-speed fighter aircraft. In order to have a good chance of capturing the vortex pair in the tower grid, the aircraft had to fly as close to the top of the towers as was feasible. In some cases, in particular the C-130E, this requirement could not be achieved. Each test site had its own tower grid geometry; that geometry -- as long as it is known -- is not critical to the reduction of the data.

## Test Sites

Tests were performed over various terrain conditions (as detailed in the tables): "Open Field" designates the cleared area at Foresthill; "Forest" designates within the tree line at Foresthill; "Orchard" denotes within the almond orchard at Chico; "Downslope" denotes the downhill terrain at Red Bluff; and "Desert" denotes the flat desert conditions at Dugway Proving Ground. Seven to ten towers were spaced uniformly apart and instrumented with propeller anemometers (tower spacing and anemometer placement were specific for each test site and are detailed in Teske 1988 and Teske, Kaufman and Curbishley 1988 and 1990). Data acquisition was housed in a command center located near the tower grid. The towers were telescoping masts (with a maximum height of 15 m) placed in a single line (with towers spaced a maximum distance of 20 m apart) normal to the anticipated aircraft flight path. The anemometers were mounted vertically at three heights above the ground (typically 5, 10 and 15 m), with three-component velocity sensors typically at two locations to capture the local ambient wind conditions prior to the test run, and after the vortices traversed the tower grid. The tower grid then presented an anemometer array that would capture on 32 propellers as much of the anticipated vortex motion as possible. As described in previous reports, once one of the aircraft vortices moved substantially off the tower grid, it became difficult for the tracking algorithm to follow the other vortex as well.

## Anemometers

Gill anemometers, manufactured by the R. M. Young Company and on loan to the USDA Forest Service from the Transportation Systems Center of the U. S. Department of Transportation, were used in all of the studies. Four-bladed propellers (19 cm in diameter) were coupled with the DC generators to complete the anemometer, and were calibrated at 1800 rpm. The anemometers were generally oriented vertically on the towers to capture the vertical velocities of the wake (avoiding the need to subtract any mean velocity). The anemometers were connected to the data acquisition system with filtering capacitors in accordance with manufacturer recommendations. The wake velocity signals were sampled

and recorded by a digital data acquisition system during the aircraft flight over the towers. Three-velocity sampling was also performed prior to each aircraft flyby to recover the ambient wind conditions.

## Data Acquisition System

The data acquisition system consisted of an IBM Portable PC with two Data Translation DT2801 auxiliary boards to sample and digitize 32 channels of analog voltage signals from the anemometers. Sampling was carried out at a rate of 100 samples per second (each anemometer was therefore sampled every 0.34 seconds). The full scale analog voltages of plus/minus 1.25 volts were converted to the digital representations 0 to 4095 and stored in computer memory. A maximum of four minutes of data could be sampled continuously, before reaching computer memory limits, and stored for post-test conversion to engineering units and further analysis. Sampling began before the aircraft flyby, to ensure sufficient ambient wind condition data.

## Test Matrix

Tables 1 through 4 summarize the data. The run numbers are Continuum Dynamics, Inc. internal numbers generated to differentiate the runs. The Status notations contain a relevant summary of each run; its various options are:

No Data: In these cases a run number was assigned but the data were not available or could not be recorded in time.

Tare Readings: In these cases the anemometer tower grid recorded a brief period of data (generally less than ten seconds) before the aircraft flybys began. These data were used to test the tower grid and contained no vortex data.

xx sec of Data: The tracking algorithm applied to this test run was able to track the vortex pair for at least xx seconds. These data were the data used to infer the previous vortex decay constant.

Marginal Data: The tracking algorithm was able to follow the vortices for a brief period of time, but the predicted time histories for the vortex pair positions and strength do not appear physical.

No Solution: The tracking algorithm could not track the vortex pair. Under the best of conditions, a numerical algorithm could not be expected to cover all of the physical possibilities during data collection. Most of the "no solution" results occurred in the almond orchard tests.

Table 1. Foresthill Run Log

| Run No. | Date | Aircraft | Location | Status |
|---|---|---|---|---|
| 1 | 06/06/85 | Bell 206B | Open Field | no data |
| 2 | | | | no data |
| 3 | | | | no data |
| 4 | | | | no data |
| 5 | | | | 20 sec of data |
| 6 | | | | no solution |
| 7 | | | | 15 sec of data |
| 8 | | | | 19 sec of data |
| 9 | | | | 28 sec of data |
| 10 | | | | 22 sec of data |
| 11 | 06/07/85 | Bell 206B | Open Field | 28 sec of data |
| 12 | | | | 25 sec of data |
| 13 | | | | no solution |
| 14 | | | | 18 sec of data |
| 15 | | | | no data |
| 16 | | | | no data |
| 17 | | | | 39 sec of data |
| 18 | | | | 59 sec of data |
| 19 | | | | no data |
| 20 | | | | 27 sec of data |
| 21 | | | | 15 sec of data |
| 22 | | | | 16 sec of data |
| 23 | | | | 12 sec of data |
| 24 | | | | marginal data |
| 25 | | | | marginal data |
| 26 | 06/08/85 | Ag Husky | Open Field | tare readings |
| 27 | | | | no data |
| 28 | | | | marginal data |
| 29 | | | | no solution |
| 30 | | | | 13 sec of data |
| 31 | | | | marginal data |
| 32 | | | | 15 sec of data |
| 33 | | | | no solution |
| 34 | | | | 16 sec of data |
| 35 | | | | 15 sec of data |
| 36 | | | | marginal data |
| 37 | | | | 15 sec of data |
| 38 | | | | 15 sec of data |
| 39 | | | | 48 sec of data |
| 40 | 06/09/85 | Ag Husky | Open Field | tare readings |
| 41 | | | | 29 sec of data |
| 42 | | | | 17 sec of data |
| 43 | | | | 12 sec of data |
| 44 | | | | 30 sec of data |
| 45 | | | | 22 sec of data |

Table 1. Foresthill Run Log (continued)

| Run No. | Date | Aircraft | Location | Status |
|---|---|---|---|---|
| 46 | 06/09/85 | Ag Husky | Open Field | 44 sec of data |
| 47 | | | | no data |
| 48 | | | | 39 sec of data |
| 49 | | | | 31 sec of data |
| 50 | | | | 23 sec of data |
| 51 | | | | 33 sec of data |
| 52 | | | | 19 sec of data |
| 53 | | | | 23 sec of data |
| 54 | | | | 22 sec of data |
| 55 | | | | no solution |
| 56 | | | | 25 sec of data |
| 57 | | | | 25 sec of data |
| 58 | | | | 33 sec of data |
| 59 | | | | 38 sec of data |
| 60 | | | | 24 sec of data |
| 61 | 06/14/85 | Bell 206B | Forest | tare readings |
| 62 | | | | 21 sec of data |
| 63 | | | | 21 sec of data |
| 64 | | | | marginal data |
| 65 | | | | 27 sec of data |
| 66 | | | | 23 sec of data |
| 67 | | | | 29 sec of data |
| 68 | | | | 26 sec of data |
| 69 | | | | 37 sec of data |
| 70 | | | | 26 sec of data |
| 71 | | | | 21 sec of data |
| 72 | | | | 26 sec of data |
| 73 | | | | marginal data |
| 74 | | | | 20 sec of data |
| 75 | 06/15/85 | Bell 206B | Forest | tare readings |
| 76 | | | | 32 sec of data |
| 77 | | | | marginal data |
| 78 | | | | marginal data |
| 79 | | | | 28 sec of data |
| 80 | | | | no solution |
| 81 | | | | 21 sec of data |
| 82 | | | | 20 sec of data |
| 83 | | | | marginal data |
| 84 | | | | 26 sec of data |
| 85 | | | | 17 sec of data |
| 86 | | | | 23 sec of data |
| 87 | | | | marginal data |
| 88 | | | | 14 sec of data |
| 89 | | | | 25 sec of data |
| 90 | | | | 34 sec of data |
| 91 | | | | 32 sec of data |

Table 1. Foresthill Run Log (continued)

| Run No. | Date | Aircraft | Location | Status |
|---|---|---|---|---|
| 92 | 06/15/85 | Bell 206B | Forest | 23 sec of data |
| 93 | | | | 11 sec of data |
| 94 | | | | no solution |
| 95 | | | | 33 sec of data |
| 96 | | | | 12 sec of data |
| 97 | | | | 26 sec of data |
| 98 | | | | 33 sec of data |
| 99 | 06/16/85 | Ag Husky | Forest | tare readings |
| 100 | | | | tare readings |
| 101 | | | | marginal data |
| 102 | | | | 25 sec of data |
| 103 | | | | marginal data |
| 104 | | | | no solution |
| 105 | | | | no solution |
| 106 | | | | marginal data |
| 107 | | | | no solution |
| 108 | | | | marginal data |
| 109 | | | | no solution |
| 110 | | | | marginal data |
| 111 | | | | no solution |
| 112 | | | | 13 sec of data |
| 113 | | | | marginal data |
| 114 | | | | 25 sec of data |
| 115 | | | | no solution |
| 116 | | | | marginal data |
| 117 | | | | 27 sec of data |
| 118 | 06/17/85 | Ag Husky | Forest | tare readings |
| 119 | | | | 48 sec of data |
| 120 | | | | 16 sec of data |
| 121 | | | | 38 sec of data |
| 122 | | | | 25 sec of data |
| 123 | | | | 40 sec of data |
| 124 | | | | 25 sec of data |
| 125 | | | | 19 sec of data |
| 126 | | | | 25 sec of data |
| 127 | | | | 45 sec of data |
| 128 | | | | 22 sec of data |
| 129 | | | | marginal data |
| 130 | | | | 232 sec of data |
| 131 | | | | 26 sec of data |
| 132 | | | | marginal data |
| 133 | | | | 15 sec of data |
| 134 | | | | 30 sec of data |
| 135 | | | | 30 sec of data |
| 136 | | | | 25 sec of data |

Table 2. Chico Run Log

| Run No. | Date | Aircraft | Location | Status |
|---|---|---|---|---|
| 1 | 06/24/85 | Ag Cat | Orchard | no data |
| 2 | | | | tare readings |
| 3 | | | | no solution |
| 4 | | | | no solution |
| 5 | | | | 17 sec of data |
| 6 | | | | marginal data |
| 7 | | | | no solution |
| 8 | | | | 34 sec of data |
| 9 | | | | no data |
| 10 | | | | tare readings |
| 11 | | | | no solution |
| 12 | | | | marginal data |
| 13 | | | | marginal data |
| 14 | | | | no solution |
| 15 | | | | no solution |
| 16 | | | | no solution |
| 17 | | | | no data |
| 18 | 06/26/85 | Ag Cat | Orchard | tare readings |
| 19 | | | | 38 sec of data |
| 20 | | | | 22 sec of data |
| 21 | | | | marginal data |
| 22 | | | | no data |
| 23 | | | | tare readings |
| 24 | | | | no solution |
| 25 | | | | 14 sec of data |
| 26 | | | | 21 sec of data |
| 27 | | | | 30 sec of data |
| 28 | | | | marginal data |
| 29 | | | | no solution |
| 30 | | | | no data |
| 31 | | | | tare readings |
| 32 | | | | 32 sec of data |
| 33 | | | | marginal data |
| 34 | | | | 28 sec of data |
| 35 | | | | 42 sec of data |
| 36 | | | | 35 sec of data |
| 37 | | | | 39 sec of data |
| 38 | | | | no solution |
| 39 | | | | no data |
| 40 | 06/28/85 | Hiller 12E | Orchard | tare readings |
| 41 | | | | no data |
| 42 | | | | tare readings |
| 43 | | | | 29 sec of data |
| 44 | | | | tare readings |
| 45 | | | | 26 sec of data |
| 46 | | | | 27 sec of data |

Table 2. Chico Run Log (continued)

| Run No. | Date | Aircraft | Location | Status |
|---|---|---|---|---|
| 47 | 06/28/85 | Hiller 12E | Orchard | 22 sec of data |
| 48 | | | | 15 sec of data |
| 49 | | | | 12 sec of data |
| 50 | | | | 26 sec of data |
| 51 | | | | 30 sec of data |
| 52 | | | | no solution |
| 53 | | | | no data |
| 54 | | | | tare readings |
| 55 | | | | marginal data |
| 56 | | | | marginal data |
| 57 | | | | 22 sec of data |
| 58 | | | | marginal data |
| 59 | | | | no solution |
| 60 | | | | no solution |
| 61 | | | | 29 sec of data |
| 62 | | | | 29 sec of data |
| 63 | | | | 21 sec of data |
| 64 | | | | no data |
| 65 | 07/02/85 | Hiller 12E | Orchard | tare readings |
| 66 | | | | no data |
| 67 | | | | tare readings |
| 68 | | | | no solution |
| 69 | | | | tare readings |
| 70 | | | | 15 sec of data |
| 71 | | | | no solution |
| 72 | | | | no solution |
| 73 | | | | no solution |
| 74 | | | | no solution |
| 75 | | | | 13 sec of data |
| 76 | | | | 12 sec of data |
| 77 | | | | no solution |
| 78 | | | | no solution |
| 79 | | | | no data |
| 80 | | | | tare readings |
| 81 | | | | 25 sec of data |
| 82 | | | | 17 sec of data |
| 83 | | | | no solution |
| 84 | | | | 20 sec of data |
| 85 | | | | tare readings |
| 86 | | | | no solution |
| 87 | | | | no solution |
| 88 | | | | marginal data |
| 89 | | | | marginal data |
| 90 | | | | no solution |
| 91 | | | | no solution |
| 92 | | | | no data |

Table 2. Chico Run Log (continued)

| Run No. | Date | Aircraft | Location | Status |
|---|---|---|---|---|
| 93 | 07/04/85 | Hiller 12E | Orchard | tare readings |
| 94 | | | | no data |
| 95 | | | | tare readings |
| 96 | | | | 32 sec of data |
| 97 | | | | 28 sec of data |
| 98 | | | | 25 sec of data |
| 99 | | | | tare readings |
| 100 | | | | 32 sec of data |
| 101 | | | | 27 sec of data |
| 102 | | | | 27 sec of data |
| 103 | | | | tare readings |
| 104 | | | | 31 sec of data |
| 105 | | | | marginal data |
| 106 | | | | marginal data |
| 107 | | | | tare readings |
| 108 | | | | no solution |
| 109 | | | | no solution |
| 110 | | | | no solution |
| 111 | | | | 25 sec of data |
| 112 | | | | 38 sec of data |
| 113 | | | | 34 sec of data |
| 114 | 07/04/85 | Ag Cat | Orchard | no data |
| 115 | | | | tare readings |
| 116 | | | | no data |
| 117 | | | | 22 sec of data |
| 118 | | | | no solution |
| 119 | | | | no solution |
| 120 | | | | 25 sec of data |
| 121 | | | | 21 sec of data |
| 122 | | | | no solution |
| 123 | | | | no solution |
| 124 | | | | no data |
| 125 | | | | marginal data |
| 126 | | | | 27 sec of data |
| 127 | | | | no data |
| 128 | | | | tare readings |
| 129 | | | | 19 sec of data |
| 130 | | | | 19 sec of data |
| 131 | | | | 24 sec of data |
| 132 | | | | no data |
| 133 | 07/06/85 | Hiller 12E | Orchard | tare readings |
| 134 | | | | no data |
| 135 | | | | tare readings |
| 136 | | | | 27 sec of data |
| 137 | | | | no solution |
| 138 | | | | marginal data |

Table 2. Chico Run Log (continued)

| Run No. | Date | Aircraft | Location | Status |
|---|---|---|---|---|
| 139 | 07/06/85 | Hiller 12E | Orchard | 16 sec of data |
| 140 | | | | 15 sec of data |
| 141 | | | | 19 sec of data |
| 142 | | | | no solution |
| 143 | | | | no data |

Table 3. Red Bluff Run Log

| Run No. | Date | Aircraft | Location | Status |
|---|---|---|---|---|
| 1 | 04/27/86 | C-130E | Downslope | marginal data |
| 2 | | | | no solution |
| 3 | | | | no solution |
| 4 | | | | 24 sec of data |
| 5 | 04/28/86 | Bell 206B | Downslope | 40 sec of data |
| 6 | | | | 99 sec of data |
| 7 | | | | marginal data |
| 8 | 04/29/86 | Bell 206B | Downslope | marginal data |
| 9 | | | | 64 sec of data |
| 10 | | | | 31 sec of data |
| 11 | | | | marginal data |
| 12 | | | | marginal data |
| 13 | | | | marginal data |
| 14 | 04/30/86 | Bell 206B | Downslope | marginal data |
| 15 | | | | 19 sec of data |
| 16 | | | | 21 sec of data |
| 17 | | | | 15 sec of data |
| 18 | | | | 66 sec of data |
| 19 | | | | 36 sec of data |
| 20 | 05/01/86 | Bell 206B | Downslope | marginal data |
| 21 | 05/04/86 | Bell 206B | Downslope | 32 sec of data |
| 22 | | | | marginal data |
| 23 | | | | marginal data |
| 24 | | | | 46 sec of data |
| 25 | | | | 33 sec of data |
| 26 | | | | 80 sec of data |
| 27 | | | | marginal data |
| 28 | | | | 67 sec of data |
| 29 | | | | 45 sec of data |
| 30 | | | | 67 sec of data |
| 31 | | | | 83 sec of data |
| 32 | | | | 59 sec of data |
| 33 | | | | 32 sec of data |
| 34 | | | | marginal data |
| 35 | | | | 17 sec of data |
| 36 | | | | 45 sec of data |
| 37 | | | | 16 sec of data |
| 38 | | | | 25 sec of data |
| 39 | 05/07/86 | Bell 206B | Downslope | 26 sec of data |
| 40 | | | | 53 sec of data |
| 41 | | | | marginal data |
| 42 | | | | 58 sec of data |

Table 3. Red Bluff Run Log (continued)

| Run No. | Date | Aircraft | Location | Status |
|---|---|---|---|---|
| 43 | 05/08/86 | Bell 206B | Downslope | marginal data |
| 44 | | | | 90 sec of data |
| 45 | | | | marginal data |
| 46 | | | | 40 sec of data |
| 47 | | | | marginal data |
| 48 | | | | 11 sec of data |
| 49 | | | | 14 sec of data |

Table 4. Dugway Run Log

| Run No. | Date | Aircraft | Location | Status |
|---|---|---|---|---|
| 1 | 10/03/88 | F-4 | Desert | 22 sec of data |
| 2 | | | | 30 sec of data |
| 3 | | | | no data |
| 4 | | | | 40 sec of data |
| 5 | | | | 60 sec of data |
| 6 | | | | 20 sec of data |
| 7 | | | | 25 sec of data |
| 8 | | | | 30 sec of data |
| 9 | | | | 34 sec of data |
| 10 | | | | 50 sec of data |
| 11 | | | | 35 sec of data |
| 12 | | | | 40 sec of data |
| 13 | | | | 40 sec of data |
| 14 | | | | 40 sec of data |
| 15 | | | | 30 sec of data |
| 16 | | | | 30 sec of data |
| 1 | 10/15/90 | F-16 | Desert | 35 sec of data |
| 2 | | | | 20 sec of data |
| 3 | | | | 30 sec of data |
| 4 | | | | marginal data |
| 5 | | | | marginal data |
| 6 | | | | 50 sec of data |
| 7 | | | | 30 sec of data |
| 8 | | | | 40 sec of data |
| 9 | | | | 30 sec of data |
| 10 | | | | no data |
| 11 | | | | marginal data |
| 12 | | | | 45 sec of data |
| 13 | | | | 65 sec of data |
| 14 | | | | 45 sec of data |
| 15 | | | | marginal data |
| 16 | 10/26/90 | F-15 | Desert | marginal data |
| 17 | | | | 20 sec of data |
| 18 | | | | 40 sec of data |
| 19 | | | | marginal data |
| 20 | | | | 30 sec of data |
| 21 | | | | 50 sec of data |
| 22 | | | | 45 sec of data |
| 23 | | | | 60 sec of data |
| 24 | | | | no data |
| 25 | | | | 50 sec of data |
| 26 | | | | 45 sec of data |
| 27 | | | | no data |
| 28 | | | | 45 sec of data |
| 29 | | | | 30 sec of data |

# 3. TRACKING ALGORITHM

An aircraft wake may be represented by a simple vortex pair (with its image pair below the surface as shown in Figure 1), each vortex of which may be characterized by a velocity field of the form

$$v = \frac{\Gamma}{2\pi} \frac{R}{(R_c^2 + R^2)} \tag{1}$$

where

- $v$ = tangential velocity
- $\Gamma$ = vortex circulation strength
- $R$ = radius from vortex center
- $R_c$ = vortex core radius (taken as 0.15 m in all that follows)

The resultant velocity at any point in the flow field (and, in particular, at an anemometer location) is then the algebraic sum of the velocity contributions from the four vortices acting on the flow (the two wingtip vortices and their images). The aircraft vortex pair is located in a coordinate system relative to the tower grid, as shown in Figure 2. In its most general sense, the wake model introduces five unknowns that must be deduced from the data in any run at any time at which data are collected

- $\Gamma$ = vortex circulation strength of the upwind vortex
- $c$ = factor multiplying the vortex circulation strength of the upwind vortex to recover the vortex circulation strength of the downwind vortex
- $h$ = height of the vortex pair above the surface
- $s$ = semispan of the vortex pair (the half distance between their centers)
- $d$ = offset distance of the aircraft centerline from the assumed zero position of the anemometer tower grid

Generally speaking, as the vortices descend toward the ground (and through the tower grid), vortex circulation strength recorded by the anemometers should increase from zero to a maximum value, then decay due to diffusion by atmospheric turbulence. Its maximum value depends on the weight of the aircraft and its flight speed past the tower grid. In practical terms, however, the anemometer data can be processed without regard to the aircraft generating the data.

With different strength vortices, the line traced between the upwind and downwind vortex centers may in fact skew off horizontal; however, this feature of the flow field is not modeled as it would be extremely cumbersome and unnecessary relative to the accuracy of the field data. Because aircraft wake physics are only approximated by the simple velocity law given in Eq 1, the intent of the present analysis to seek a solution minimizing the error in the velocity predictions across many anemometer locations seems appropriate.

With five unknowns and many more anemometer locations, the problem may be cast into a least squares analysis by defining an error E such that

$$E = \sum_{n=1}^{N} (w_n - \overline{w}_n)^2 \tag{2}$$

where the overbar denotes the data, and the index n is from 1 to N, the total number of anemometers. The error E is a positive definite quantity. The vertical velocities $w_n$ are determined by summing the contributions of the four vortices in the model, calculated for specific values of the parameters $\Gamma$, c, h, s and d. The upwind vortex strength $\Gamma$ is used to compute the upwind vortex (and its image) contribution to $w_n$; the downwind vortex strength $c\Gamma$ is used to compute the downwind vortex (and its image) contribution to $w_n$. The data $\overline{w}_n$ are found directly from the test data.

A crucial physical observation is made at this point: if the experimental data were normalized by any positive value, the resulting velocity vectors could still be used to infer the spatial position of the vortex pair in the anemometer field irrespective of the actual vortex circulation strength. This observation implies that locating the vortex pair involves the solution for c, h, s and d without regard to the value of $\Gamma$.

It becomes quickly apparent, also, that the inclusion of the parameter c complicates the solution procedure tremendously; thus, we choose to select a value for c, converge on a solution for h, s and d, then modify c and repeat the convergence, all in an attempt to improve (reduce) the solution error E. In this way the original tracking algorithm remains intact at the core of the solution.

The approach used here normalizes the vertical velocities in the error equation by their respective root mean square velocities (with the assumption that the rms velocities should be the same if the solution is tracking the data accurately) to give

$$E^* = \sum \left[ \frac{w_{nu} + c\, w_{nd}}{w_{rms}} - \frac{\overline{w}_n}{\overline{w}_{rms}} \right]^2 \tag{3}$$

where

$$w_{rms} = \sqrt{\frac{1}{N} \sum (w_{nu} + c\, w_{nd})^2} \tag{4}$$

$$\overline{w}_{rms} = \sqrt{\frac{1}{N} \sum \overline{w}_n^2} \tag{5}$$

and $w_{nu}$ and $w_{nd}$ are the vertical velocity contributions from the upwind and downwind vortices, respectively.

Because the predicted vertical velocities are linear in vortex circulation strength $\Gamma$ (from Eq 1), and the parameter c is found by iteration on an outer loop of the tracking

algorithm, this modification to the error recasts the problem into one involving the three parameters h, s and d. These parameters are found by differentiating Eq 3 with respect to h, s and d to form

$$F_h = \frac{\partial E^*}{\partial h} \qquad F_s = \frac{\partial E^*}{\partial s} \qquad F_d = \frac{\partial E^*}{\partial d} \tag{6}$$

Clearly, when all three derivatives in Eq 6 tend to zero, the slope of E* also tends to zero, and E* approaches a local minimum. Local values of $F_h$, $F_s$ and $F_d$ may be determined analytically to generate influence coefficients of the form $\partial F/\partial h$, $\partial F/\partial s$ and $\partial F/\partial d$ to construct the model equation for F (representing $F_h$, $F_s$ and $F_d$) of the form

$$\Delta F = \frac{\partial F}{\partial h}\Delta h + \frac{\partial F}{\partial s}\Delta s + \frac{\partial F}{\partial d}\Delta d \tag{7}$$

Since the solution for minimum E* requires F to tend to zero, the left hand side of Eq 7 may be specified by

$$\Delta F = - F \tag{8}$$

The complete system then becomes a three-equation system for the values $\Delta h$, $\Delta s$ and $\Delta d$ to add to the present values h, s and d to give new values $h+\Delta h$, $s+\Delta s$ and $d+\Delta d$ to recompute E* and drive the solution to a minimum. Once a minimum has been reached, c is varied to find a smaller minimum and converge to a better solution. After this procedure is completed, the original error E may be differentiated to give the linear equation

$$F_\Gamma = \frac{\partial E^*}{\partial \Gamma} = 0 \tag{9}$$

to find the minimum of E and determine $\Gamma$. With the complete solution in hand at the present time step, these values are used as initial guesses for the next time step in the data run being analyzed.

A typical result is shown in Figure 3, plotting the horizontal and vertical positions of the vortices, the circulation strength of the upwind vortex, and the multiplicative factor c on the downwind vortex. A time of 0 seconds in these figures denotes the initiation of data collection just prior to aircraft flyover.

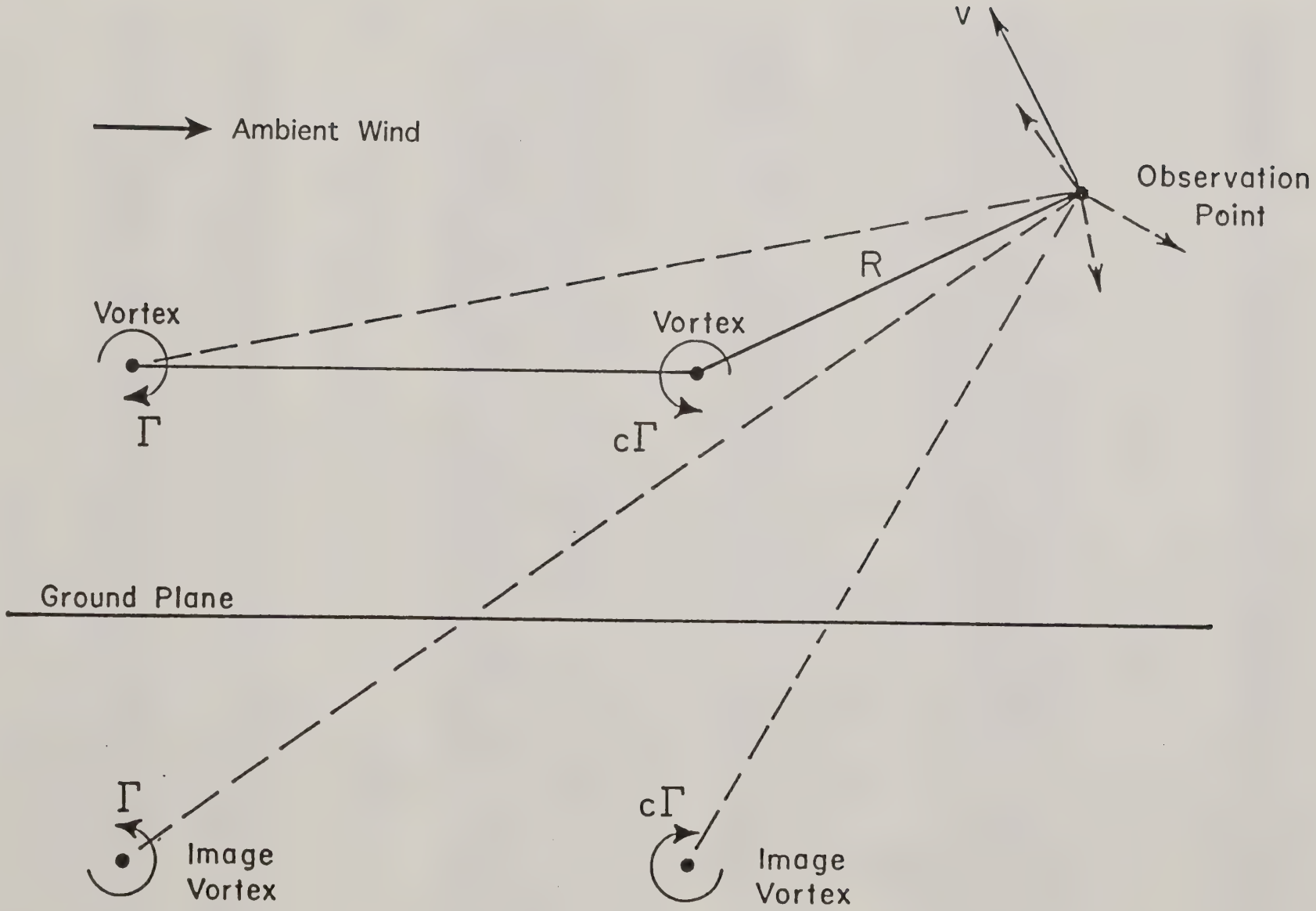


Figure 1. The composite velocity vector at an observation point found by summing the contributions of the aircraft vortex pair and its image system below the ground plane.

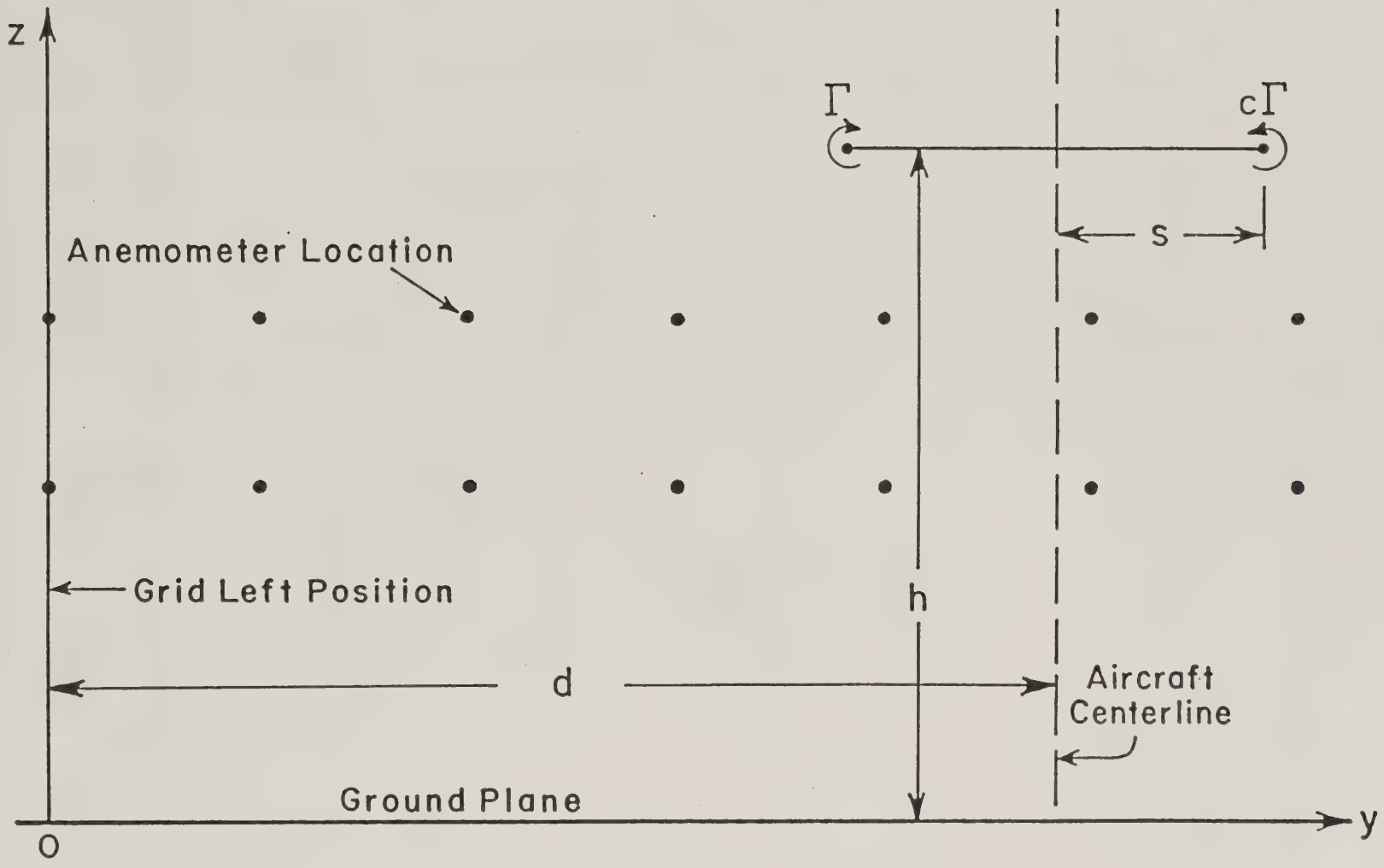


Figure 2. The aircraft vortex pair located relative to the anemometer tower grid. The relevant lengths are the height h of the vortex pair, the semispan distance s between the two vortices, and the offset d of the aircraft centerline from the grid left position at y = 0 (arbitrarily chosen).

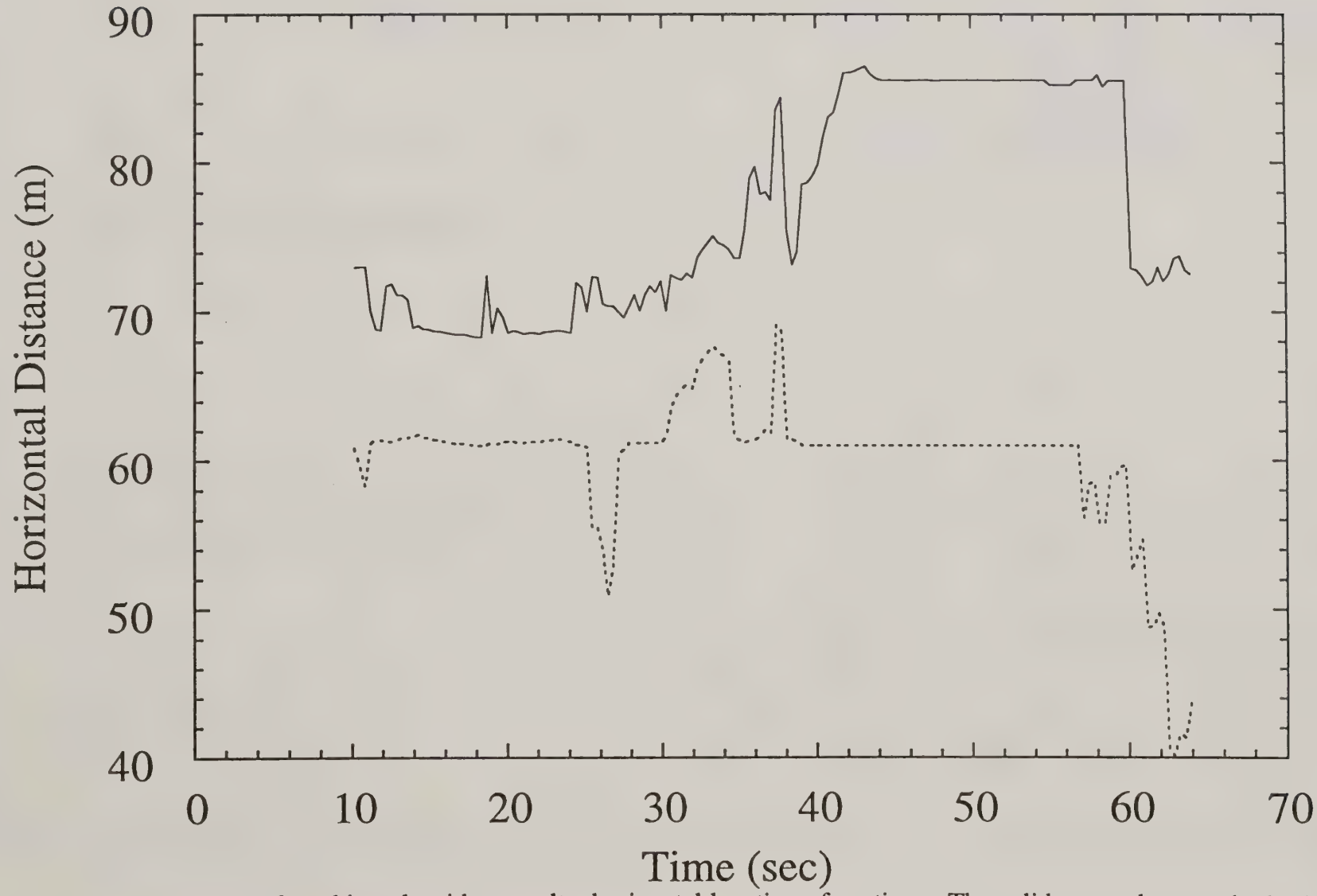


Figure 3a. Typical run of tracking algorithm results: horizontal location of vortices. The solid curve denotes the horizontal location of the downwind vortex; the dashed curve denotes the horizontal location of the upwind vortex.

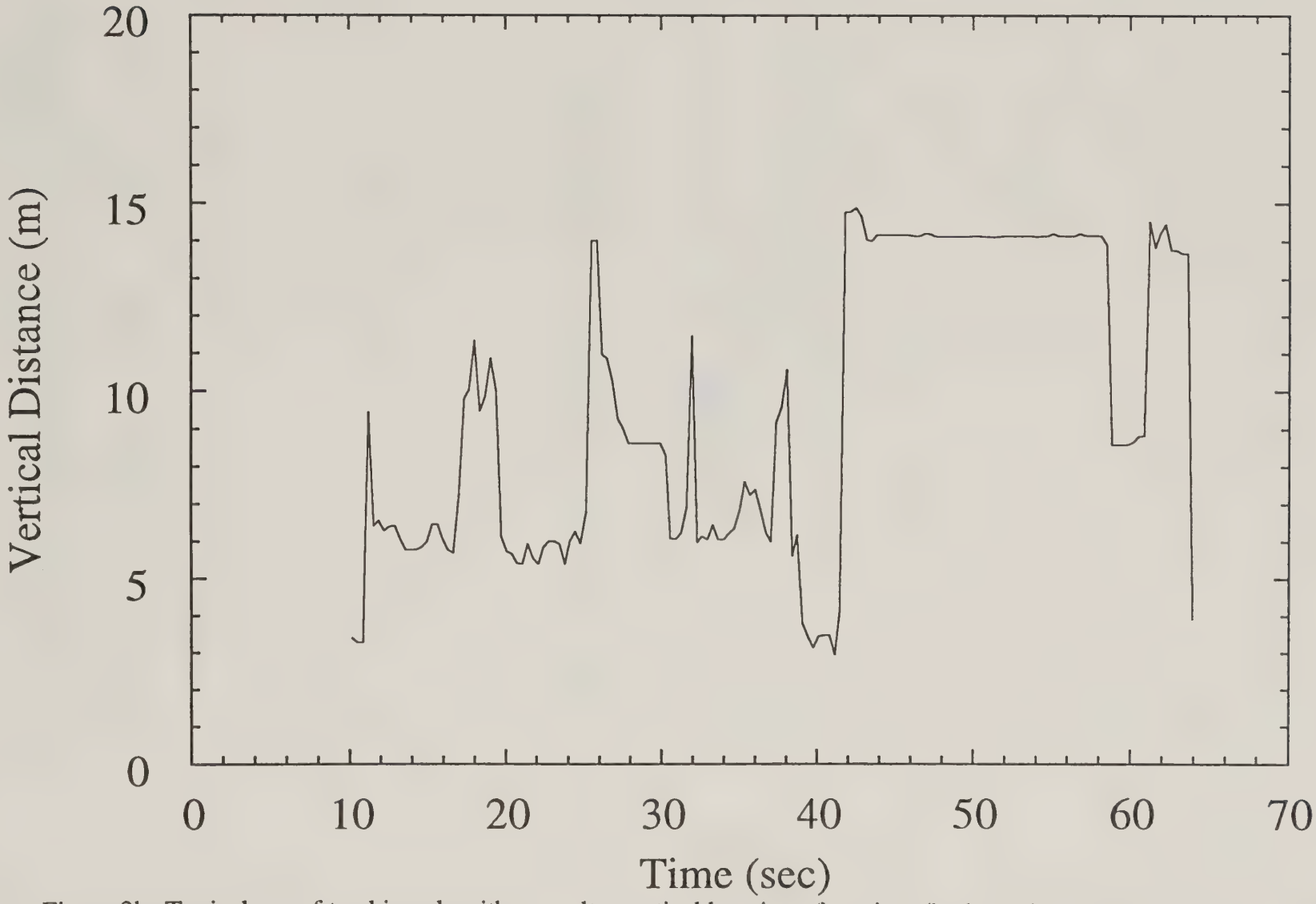


Figure 3b. Typical run of tracking algorithm results: vertical location of vortices (both vortices are at the same height).

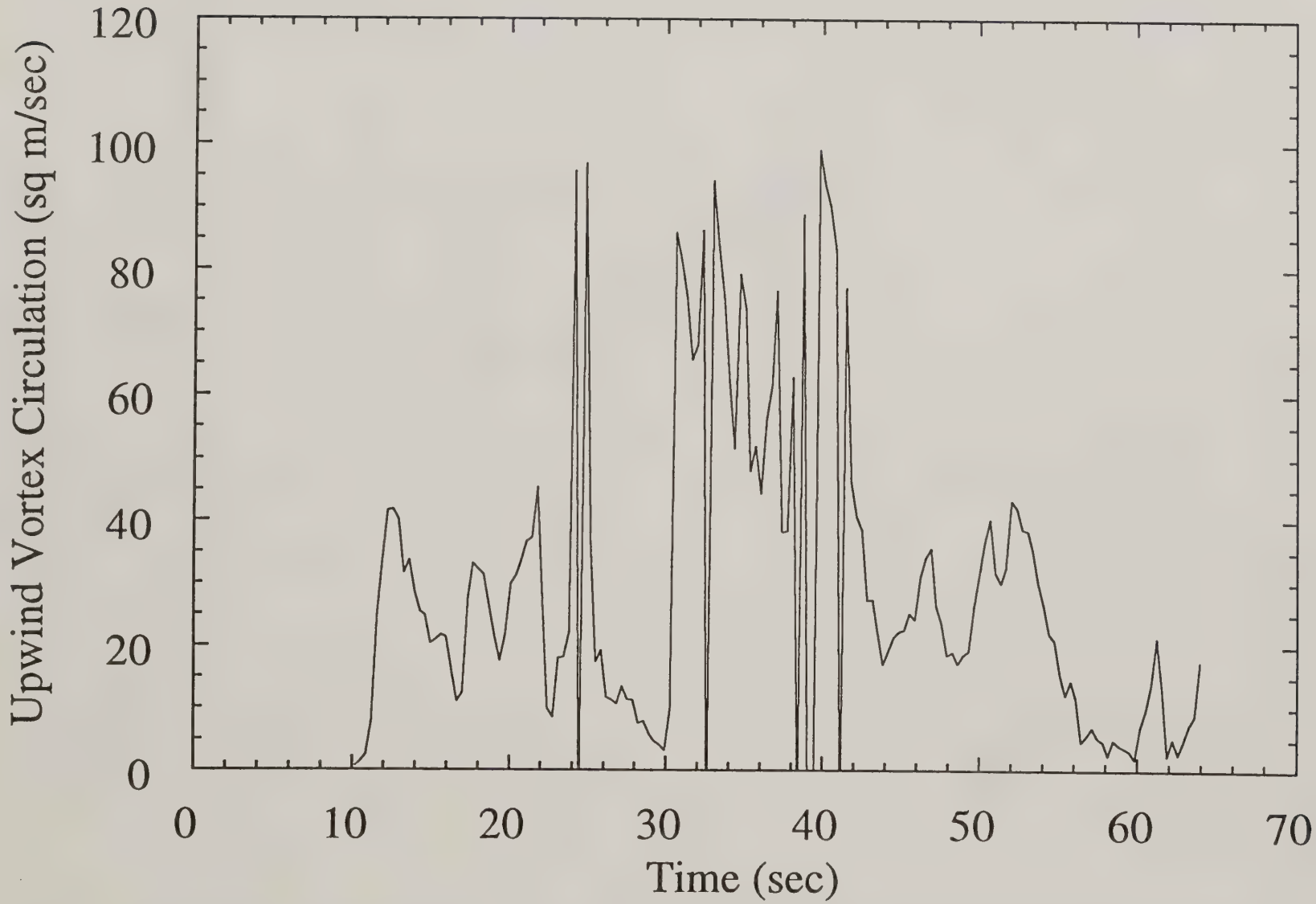


Figure 3c. Typical run of tracking algorithm results: circulation strength of upwind vortex.

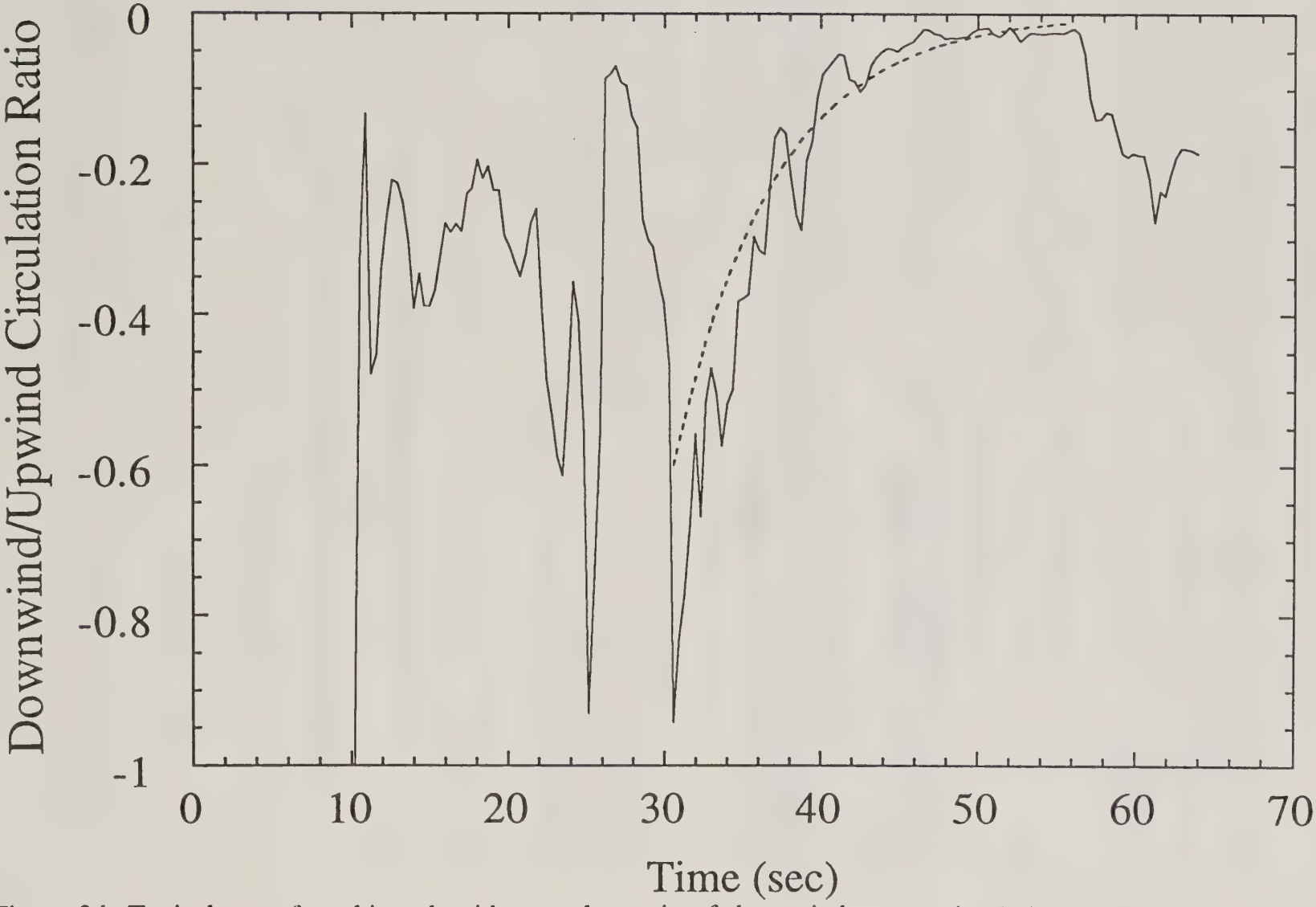


Figure 3d. Typical run of tracking algorithm results: ratio of downwind vortex circulation strength to upwind vortex circulation strength.

# 4. VORTEX DECAY EFFECT

The vortex strength decay model previously developed assumes

$$\Gamma(t) = \Gamma_0 \exp\left( - \frac{b\, q\, t}{s} \right) \tag{10}$$

where

$\Gamma$ = vortex circulation strength as a function of time t

$\Gamma_0$ = initial vortex circulation strength at t = 0 (initiation of data collection)

b = decay coefficient for the vortex pair

q = atmospheric turbulence level

s = vortex pair semispan

By least squares, the circulation results were originally fit to Eq 10, and the decay parameter bq was found to be well approximated by 0.56 m/sec (Figure 4). In the present extension to this work, we first assume that the upwind vortex follows Eq 10 (with $b = b_u$), while the downwind vortex follows

$$\Gamma(t) = \Gamma_0 \exp\left( - \frac{b_d\, q\, t}{s} \right) = c\, \Gamma_0 \exp\left( - \frac{b_u\, q\, t}{s} \right) \tag{11}$$

where we anticipate that $\Gamma_0$, $b_d$, $b_u$ and c are constants for each aircraft flyover. Combining the two expressions in Eq 11 gives

$$\ln (c) = (b_u - b_d)\, q\, t / s \tag{12}$$

If we assume that the decay parameters have the form

$$b_u = b - \Delta b \qquad b_d = b + \Delta b \tag{13}$$

then Eq 12 may be rewritten to give

$$\ln (c) = - 2\, \Delta b q\, t / s \tag{14}$$

Thus, each aircraft flyover result should be curve fit with Eq 14 to determine $\Delta bq$ and complete the analysis. The normalized crosswind may be found from the expression

$$\beta = \frac{\partial V}{\partial z} \frac{2 \pi s^2}{\Gamma_o} \qquad (15)$$

where V is the crosswind velocity and z is the height above the ground (this normalization was first introduced in Bilanin, Teske and Hirsh 1978). The linear least squares technique generates the results summarized in Figure 5 for the 156 applicable runs. Since $\Delta bq$ must equal 0.0 at $\beta = 0.0$ (to recover equal decay of the two vortices when there is no crosswind), an additional linear least squares line through the results shown in Figure 5 finds that

$$\Delta bq = 0.264\ \beta \quad \text{(m/sec)} \qquad (16)$$

as the principal finding of this research. Since the value of 0.264 m/sec is nearly half of the previously averaged decay parameter 0.56 m/sec, it may be reasonably assumed that the presence of a crosswind significantly impacts the decay rates of the upwind and downwind vortices.

A previous numerical study of a vortex pair decaying above the ground in a crosswind (Bilanin, Teske and Hirsh 1978) gives the decay behavior illustrated in Figure 6 (for, in this case, $\beta = 0.5$). Applying Eqs 10 and 14 to these predictions results in a value of $\Delta bq = 0.12$ m/sec, consistent with the experimental results given in Figure 5.

Equation 16 gives the result when the crosswind effect augments/decays at the same rate for both vortices. An even better result may be obtained by developing the decay rates for the upwind and downwind vortices separately (retaining $b_u$ and $b_d$ independently instead of making the simplifying assumption in Eq 13). In this approach the results (shown in Figure 7) become

$$b_u q = 0.56 - 0.184\ \beta \qquad \text{(upwind vortex, m/sec)} \qquad (17)$$

$$b_d q = 0.56 + 0.292\ \beta \qquad \text{(downwind vortex, m/sec)} \qquad (18)$$

These decay rates refine the previous results, and are therefore recommended.

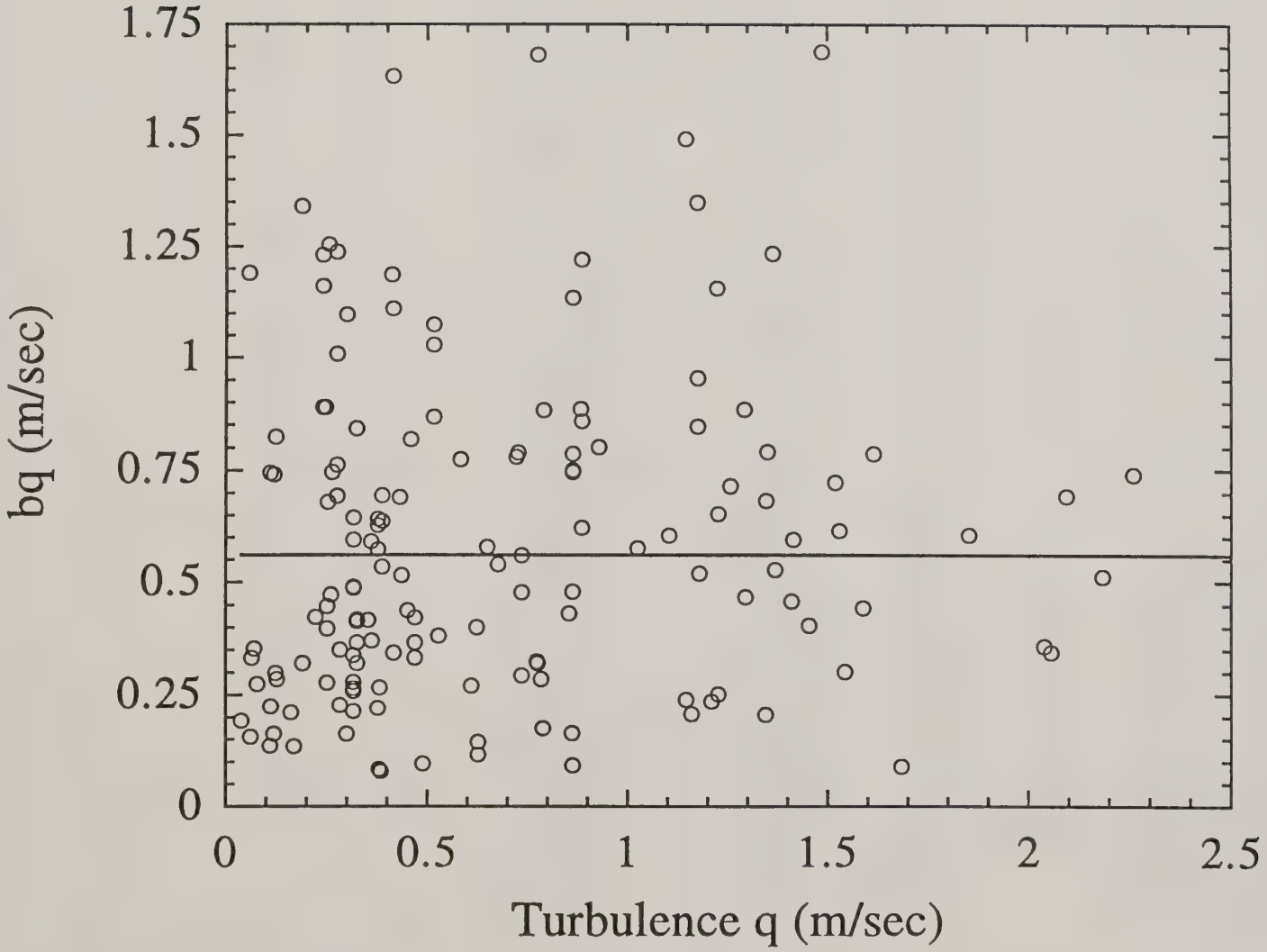


Figure 4. The behavior of the product bq with turbulence level q for all data sets. Each circle represents one of 132 applicable test runs. The solid curve is the mean of the data.

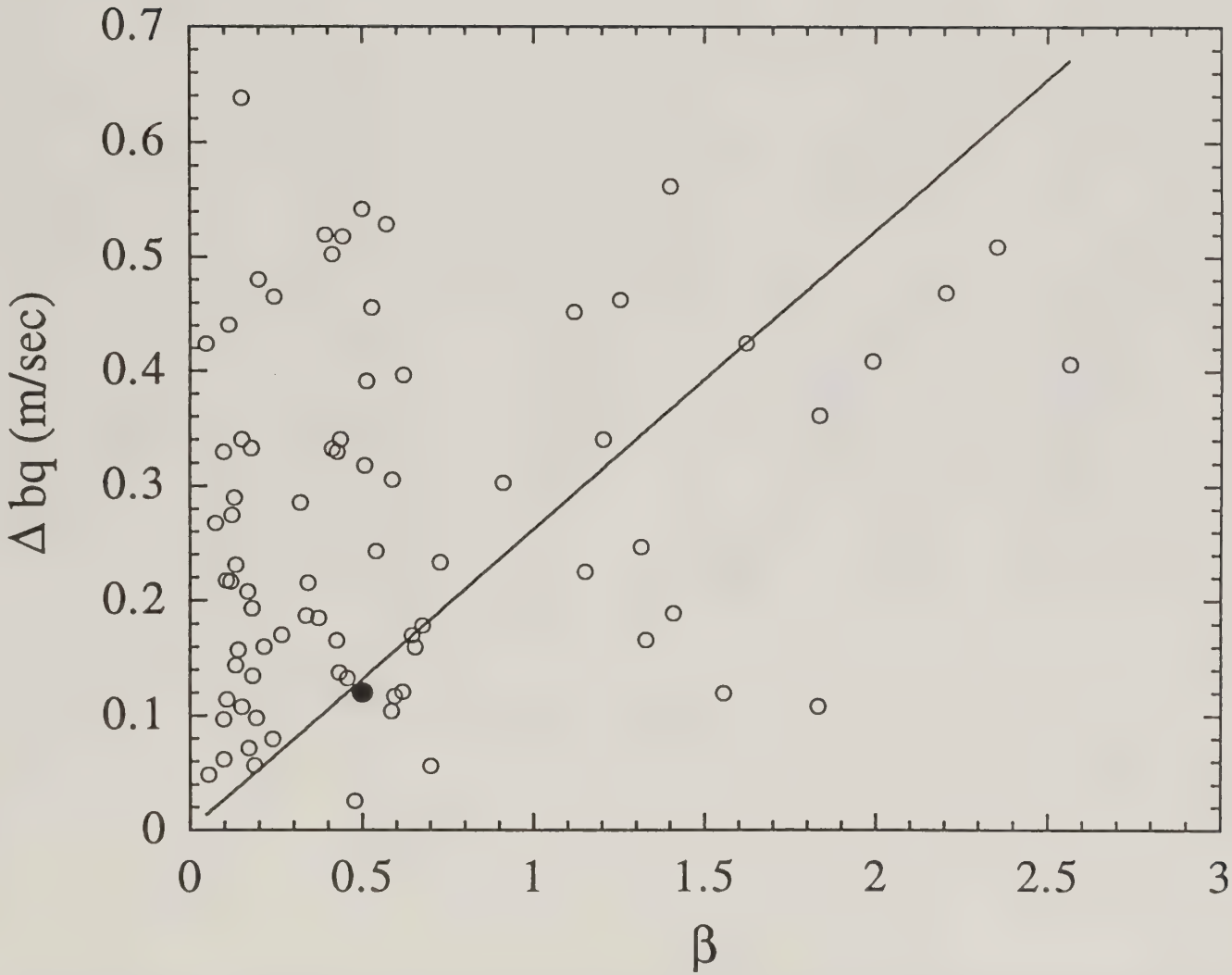


Figure 5. Correlation of vortex decay correction due to crosswind shear for all data sets. Each circle represents one of the 156 applicable test runs. The solid curve is the best slope through the data. The solid circle is an analytical result from Bilanin, Teske and Hirsh (1978).

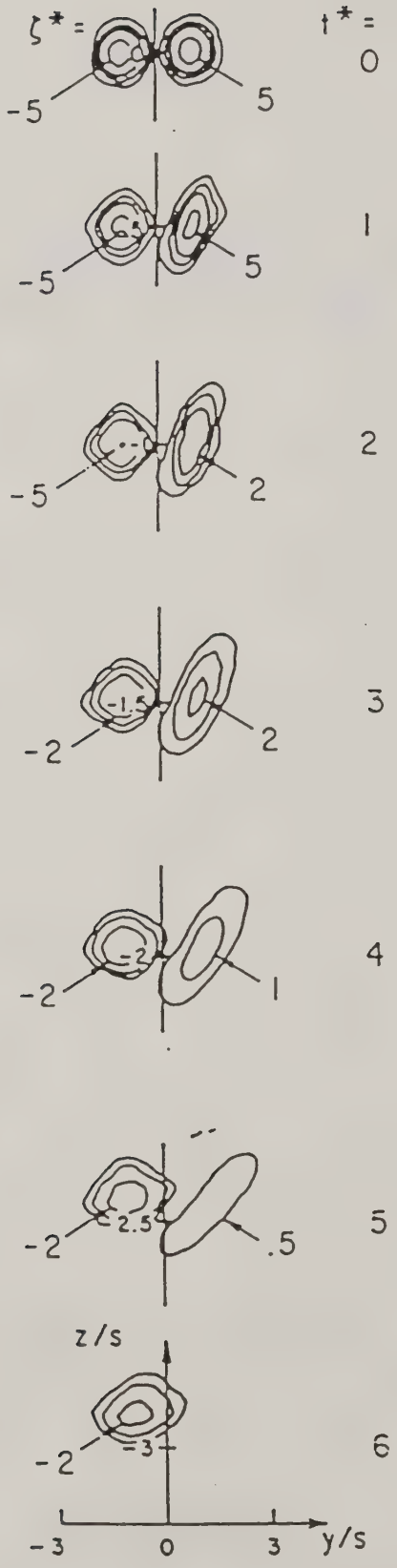


Figure 6. Isopleths of normalized vorticity $\zeta^*$ for a vortex pair subjected to a crosswind shear of $\beta = 0.5$ from the left (Bilanin, Teske and Hirsh 1978), shown as a function of normalized time t*. The crosswind shear is removed to highlight the decaying vortices.

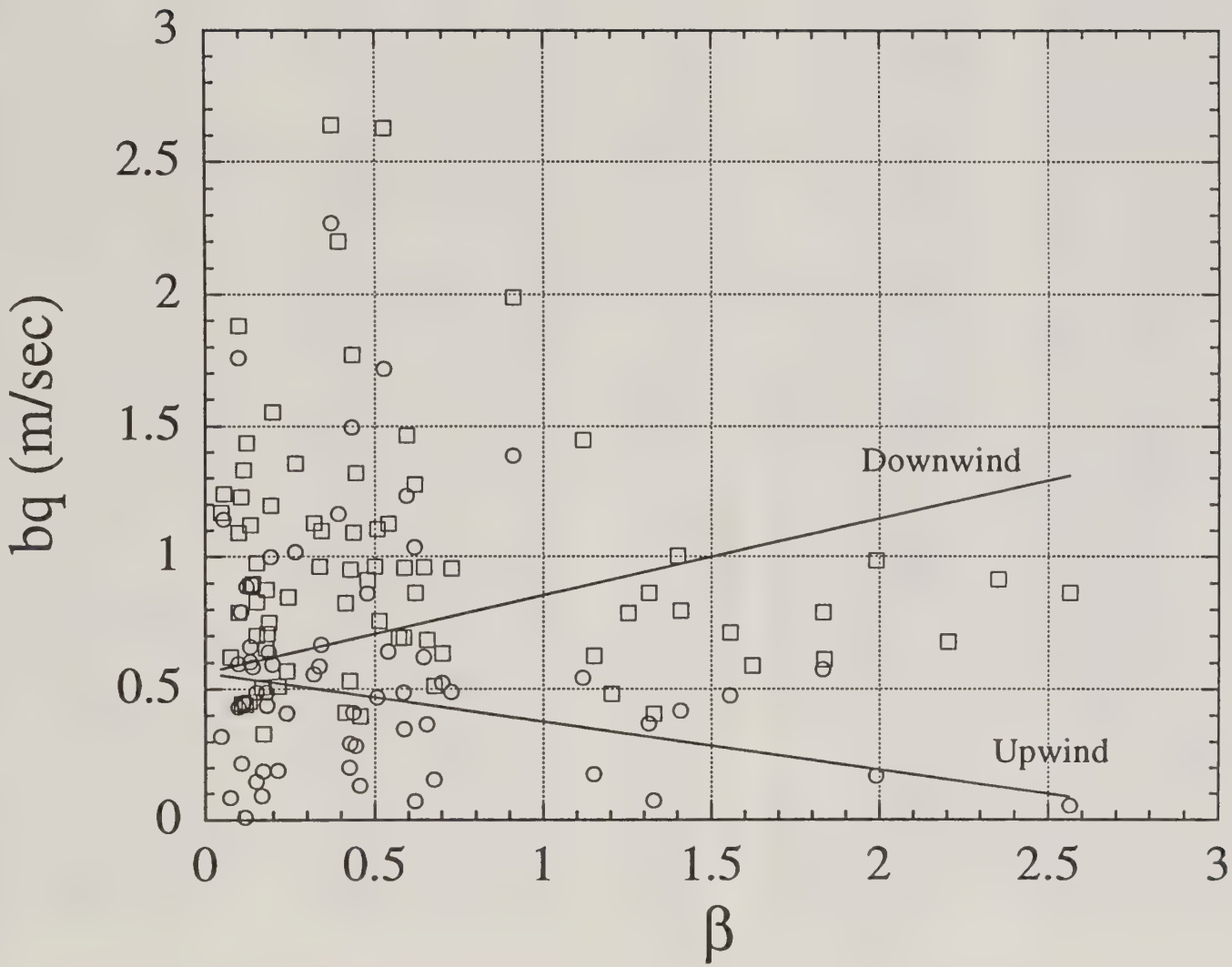


Figure 7. The behavior of the product bq with nondimensional crosswind shear β for all data sets. Each circle represents an upwind vortex; each square, a downwind vortex; with 156 applicable test runs. The solid lines are the best slopes through the upwind and downwind data, anchored at bq = 0.56 m/sec when β = 0.

# 5. FSCBG PREDICTIONS

McCooeye et al. (1993) present field data suggesting that the different vortex strength decay rates for the upwind and downwind vortices may influence the deposition pattern of aerially released material. To confirm this hypothesis, we apply the results obtained in the last section of this report and exercise the aerial spray model FSCBG modified for different vortex strength decay rates on the upwind and downwind sides of the aircraft (Eqs 17 and 18). We use the model inputs summarized in Table 5, with atomizations given in Table 6, for the conditions specified by McCooeye et al. (1993), since we believe that the observed effect is strongly dependent on aircraft type and speed, nozzle location, and atomization. Model inputs were obtained from appropriate tables in their report; however, specific drop size distributions for each of the nine field trials had to be selected from the several atomizations provided by McCooeye et al. (1993). Only mass deposition was recovered by McCooeye et al. (1993).

We initiate the model runs, separately with nozzles on the upwind side of the aircraft and with nozzles on the downwind side of the aircraft. The ground depositions out to 200 m downwind are summed (consistent with the McCooeye et al. 1993 field results), and the percent of deposit from the upwind side of the aircraft is compared to the percent of deposit from the downwind side. Both predictions are compared with the data results of McCooeye et al. (1993) in Table 7. Because of mass balance uncertainty in the data (Mickle 1995), only the deposit data are shown in Table 7.

For the most part FSCBG model predictions fall within or close to the recovery percentages suggested by the field data. In addition the data averages for upwind and downwind data and predictions are comparable. These results are very encouraging and indicate consistency between the field data and FSCBG predictions.

Recent correspondence (Young 1993 and Mickle 1993) suggest that the atomization data is still in question. Clearly, Table 6 shows that the drop size distributions inferred for the downwind atomizers carry lower volume median diameters (VMD) than the upwind atomizers, and therefore imply a finer drop spray downwind, which would naturally enhance drift from the downwind nozzles. If this were the case, the field study would tend to treat the upwind and downwind nozzles preferentially. McCooeye et al. (1993) were in fact quite surprised that the atomizations were different for the two tracers used in the trials, and suggest that the atomizations themselves may be incorrect because of high obscuration during wind tunnel examination (Mickle 1993). Their remarks, and the apparent ambiguity in drop size distributions, suggest the need for further field study.

Spray Trial 1 (from Table 7) shows perhaps the best agreement between field data and FSCBG predictions. The corresponding mass deposit profiles are shown in Figure 8, where it may be seen that the upwind nozzles contribute more deposition close to the aircraft than the downwind nozzles. A companion plot of number density (for the assumed mass size distribution which, from the above discussion, may be incorrect) is shown in Figure 9, where the exact opposite effect is seen: more drops have deposited from the downwind nozzles close to the aircraft than from the upwind nozzles. This effect comes about because the upwind vortex "captures" the smaller drops and prevents them from depositing (the larger drops contain much more of the mass). Thus, the recovery of number of drops -- in addition to mass -- is important in any field study.

These findings suggest implementation of an extended near-wake vortex model into FSCBG. That discussion follows in the next section of this report.

Table 5. FSCBG Model Inputs

| Input Parameter | Value |
|---|---|
| Aircraft Type | Cessna Ag Truck |
| Semispan | 6.35 m |
| Aircraft Weight | 13,610 N |
| Nozzle Type | Micronair AU4000 |
| Number of Nozzles | 2 on each side of aircraft |
| Nozzle Locations | ±1.52 m, ±3.53 m from aircraft centerline |
| Volatile Fraction | 0.9 |
| Normalized Flow Rate | 10.0 gm/m |

| Spray Trial Number | Wind Speed at 10 m (m/sec) | Wind Direction increment (deg) | Temperature (deg C) | Relative Humidity (percent) |
|---|---|---|---|---|
| 1 | 3.31 | 10.3 | 8 | 50 |
| 2 | 2.31 | 7.3 | 8 | 75 |
| 3 | 2.05 | 50.0 | 10 | 35 |
| 4 | 3.07 | 9.1 | 4 | 55 |
| 5 | 3.21 | 5.4 | 2 | 62 |
| 6 | 1.56 | 10.4 | 1 | 65 |
| 7 | 0.56 | 31.0 | 8 | 62 |
| 8 | 5.32 | 9.6 | 4 | 55 |
| 9 | 4.50 | 30.0 | 10 | 20 |

| Spray Trial Number | Release Height (m) | Spraying Speed (m/sec) | Upwind Drop Size | Downwind Drop Size |
|---|---|---|---|---|
| 1 | 9.2 | 49.8 | TPP1 | TBEP1 |
| 2 | 9.9 | 52.5 | TPP1 | TBEP1 |
| 3 | 28.1 | 52.5 | TPP1 | TBEP1 |
| 4 | 26.4 | 53.5 | TPP2 | TBEP1 |
| 5 | 21.9 | 52.3 | TPP2 | TBEP2 |
| 6 | 30.2 | 51.9 | TPP2 | TBEP2 |
| 7 | 8.4 | 50.1 | TPP2 | TBEP2 |
| 8 | 10.9 | 51.7 | TPP2 | TBEP3 |
| 9 | 10.1 | 50.2 | TPP2 | TBEP3 |

Table 6. Selected Drop Size Distributions

| Average Diameter (mm) | Mass Fraction TPP1 | Mass Fraction TPP2 | Mass Fraction TBEP1 | Mass Fraction TBEP2 | Mass Fraction TBEP3 |
|---|---|---|---|---|---|
| 10.77 | 0.026 | 0.054 | 0.099 | 0.107 | 0.115 |
| 16.73 | 0.014 | 0.028 | 0.047 | 0.050 | 0.053 |
| 19.39 | 0.014 | 0.031 | 0.044 | 0.048 | 0.051 |
| 22.49 | 0.013 | 0.033 | 0.039 | 0.043 | 0.045 |
| 26.05 | 0.021 | 0.038 | 0.047 | 0.052 | 0.053 |
| 30.21 | 0.030 | 0.039 | 0.052 | 0.055 | 0.058 |
| 35.01 | 0.028 | 0.030 | 0.045 | 0.046 | 0.049 |
| 40.57 | 0.021 | 0.025 | 0.038 | 0.038 | 0.043 |
| 47.03 | 0.021 | 0.032 | 0.048 | 0.050 | 0.057 |
| 54.50 | 0.032 | 0.053 | 0.072 | 0.082 | 0.091 |
| 63.16 | 0.048 | 0.074 | 0.091 | 0.100 | 0.109 |
| 73.23 | 0.062 | 0.085 | 0.095 | 0.098 | 0.101 |
| 84.85 | 0.072 | 0.086 | 0.085 | 0.078 | 0.072 |
| 98.38 | 0.079 | 0.083 | 0.070 | 0.060 | 0.047 |
| 114.11 | 0.085 | 0.077 | 0.052 | 0.045 | 0.030 |
| 132.03 | 0.087 | 0.068 | 0.036 | 0.029 | 0.011 |
| 152.93 | 0.089 | 0.058 | 0.021 | 0.013 | 0.008 |
| 177.68 | 0.083 | 0.051 | 0.008 | 0.003 | 0.005 |
| 205.70 | 0.064 | 0.030 | 0.007 | 0.003 | 0.001 |
| 238.45 | 0.047 | 0.011 | 0.004 | | 0.001 |
| 276.48 | 0.029 | 0.009 | | | |
| 320.60 | 0.019 | 0.004 | | | |
| 371.65 | 0.010 | 0.001 | | | |
| 430.43 | 0.003 | | | | |
| 498.90 | 0.001 | | | | |
| 578.40 | 0.001 | | | | |
| 670.56 | 0.001 | | | | |
| VMD (μm) | 109.3 | 75.7 | 55.0 | 51.5 | 47.5 |

Table 7. Percentage of Released Spray Material Deposited to 200 m Downwind

| Spray Trial Number | FSCBG Upwind Nozzles (%) | FSCBG Downwind Nozzles(%) | Deposit Data Upwind Nozzles(%) | Deposit Data Downwind Nozzles (%) |
|---|---|---|---|---|
| 1 | 50 | 35 | 58 | 41 |
| 2 | 61 | 39 | 67 | 40 |
| 3 | 34 | 9 | 17 | 11 |
| 4 | 11 | 5 | 29 | 21 |
| 5 | 10 | 7 | 30 | 17 |
| 6 | 11 | 3 | 34 | 23 |
| 7 | 80 | 74 | 31 | 32 |
| 8 | 24 | 12 | 51 | 25 |
| 9 | 15 | 12 | 20 | 24 |
| Average | 33 | 22 | 37 | 26 |

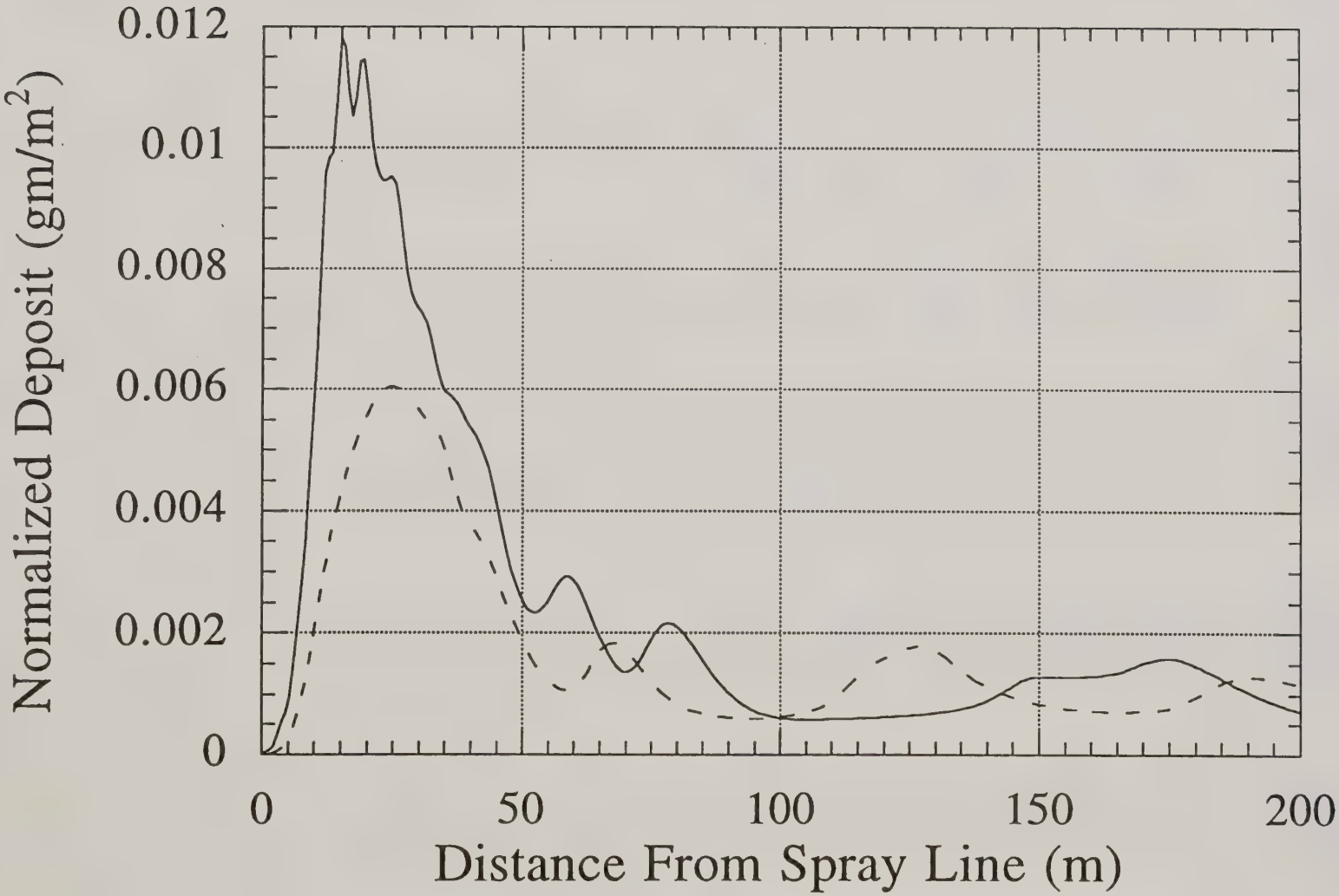


Figure 8. FSCBG mass deposit predictions from upwind nozzles (solid curve) and downwind nozzles (dashed curve) for the conditions of Spray Trial 1 given in Tables 5 and 6. The emission rate from each side of the aircraft is normalized to 10 gm/m to correct for flow rate.

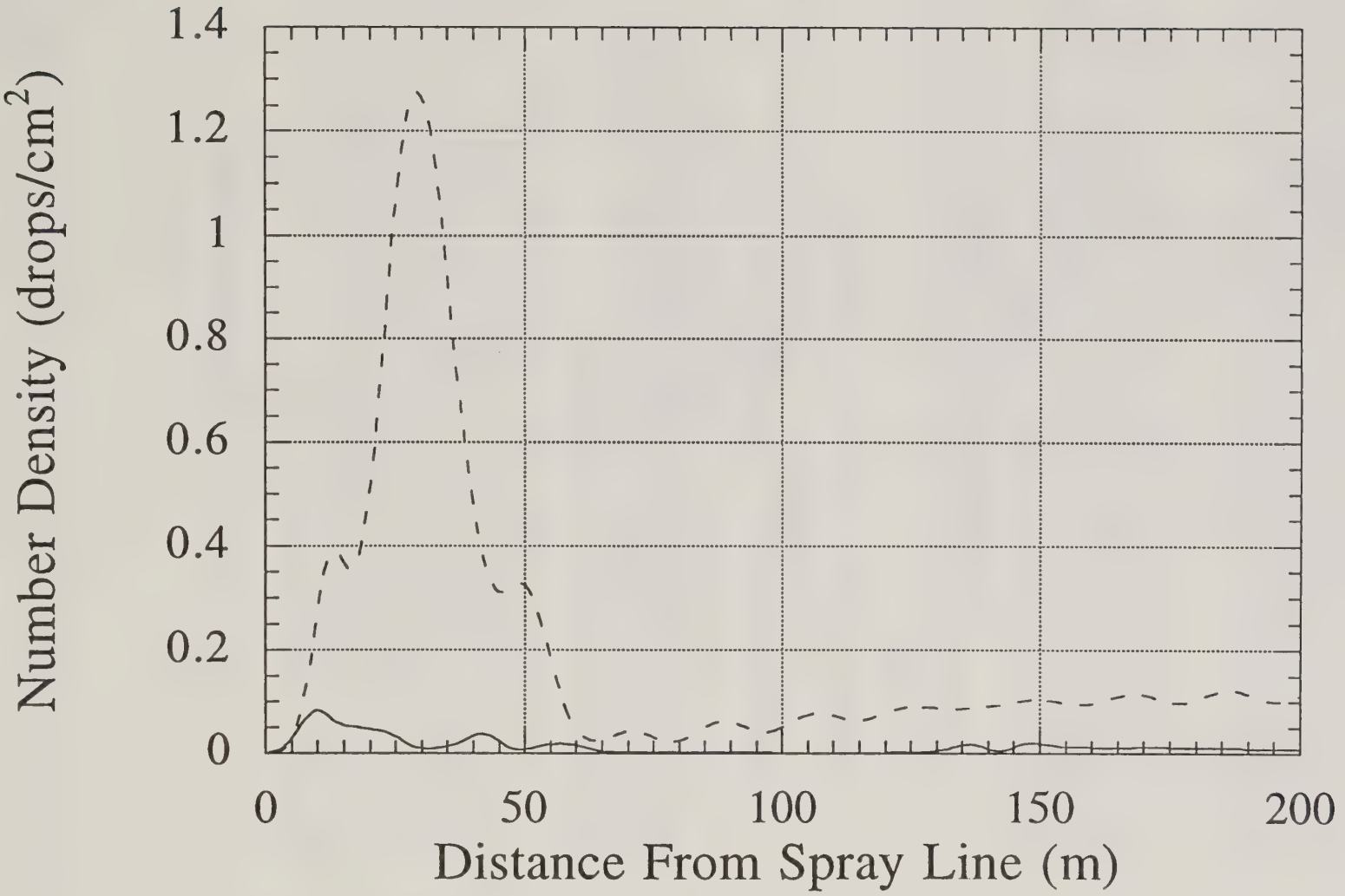


Figure 9. FSCBG number deposit predictions from upwind nozzles (solid curve) and downwind nozzles (dashed curve) for the conditions of Spray Trial 1 given in Tables 5 and 6.

# 6. MODELING CONSIDERATIONS

Equation 1 represents the wingtip vortical effect with point vortices. This approximation enables a simple representation for the vortices in the Lagrangian solution approach used in the near-wake model in FSCBG (Bilanin et al. 1989b). As the McCooeye et al. (1993) field data are repeated, this simplified approach may need to be replaced by a more accurate technique when comparing precise upwind and downwind nozzle deposition patterns. In this section of the report we address the issues raised by this observation.

We have known from the beginning of the development of the near-wake model that the Lagrangian approach was simple and fast, but could only -- at best -- generate an approximate model for the wingtip vortices. A more accurate approach is that of the Euler technique, which is far more time-consuming but better represents the physics of vortical motion near the ground. Figure 10 illustrates a typical Eulerian result (from Bilanin, Teske and Hirsh 1978) and points to the areas of difference:

1. In the Lagrangian approach the vorticity does not diffuse (spread) as it decays; instead, only a decrease in vortex strength is captured by the decay rates developed in this report.

2. Countersign vorticity off the ground is not produced.

3. The further effect of crosswind -- preferentially skewing the vortices to different heights above the ground -- is also not included.

If we were also to consider the effects of atmospheric stability on vortex motion and behavior, it is clear that the present approach contains some shortcomings, even though the current model has worked remarkably well over the years, and in fact recovers the trends suggested by the McCooeye et al. (1993) data set. A model enhancement at this point would require a new approach to the problem.

One approach that has proven successful in other applications is the use of a technique called vortex particles (Chua and Quackenbush 1992a and 1992b; Winckelmans and Leonard 1993; Chua et al. 1994). In this approach, whenever the vorticity or density equations discover an imbalance, a new point vortex particle (or density particle) is released at the required spatial location. This particle corrects the solution for the spreading of the initial vortex, the generation of countersign vorticity off the ground, the crosswind effect, and -- with density particles -- stability effects. A model of this type would be needed if a more accurate near-wake prediction is required, or if atmospheric stability needs to be modeled in a consistent fashion.

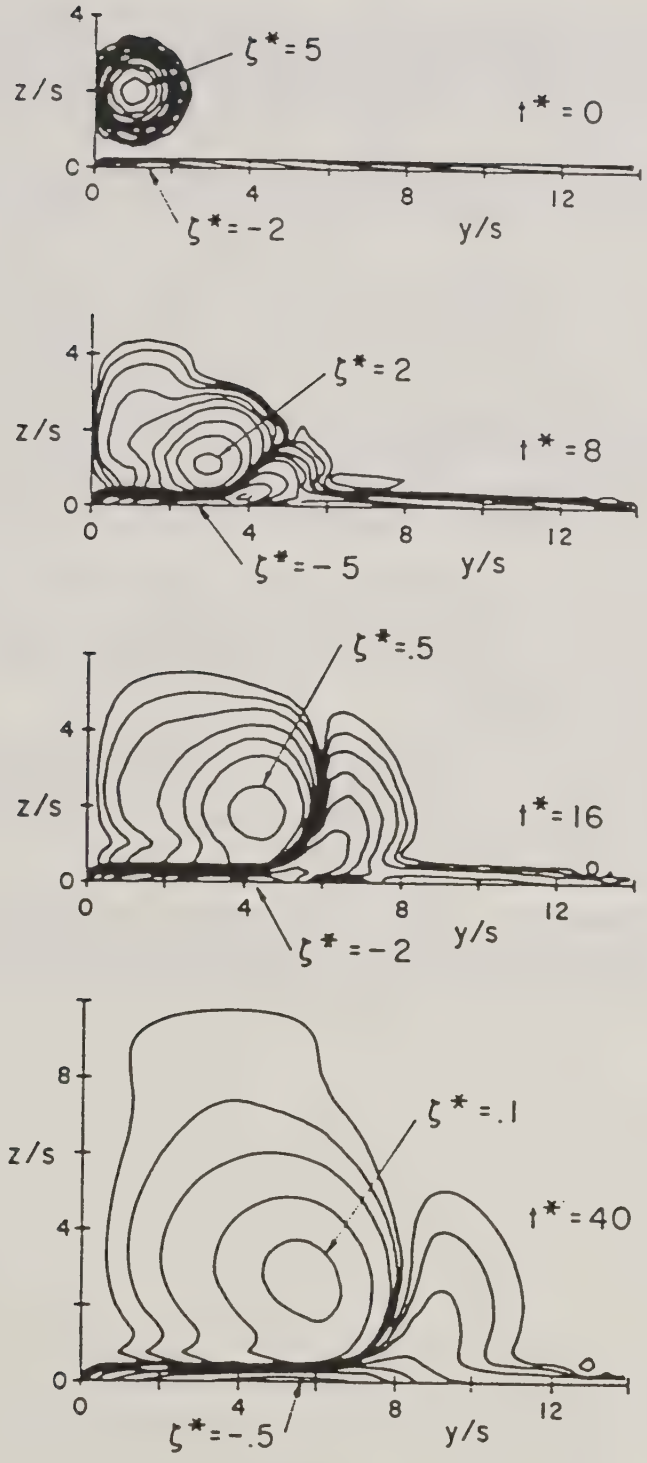


Figure 10. Isopleths of normalized vorticity $\zeta^*$ for a vortex pair descending toward the ground (Bilanin, Teske and Hirsh 1978), shown as a function of normalized time t*.

# 7. SUMMARY OF FINDINGS

Recent field studies by McCooeye et al. (1993) and Huddleston et al. (1994) suggest that spray material released from downwind nozzles tend to drift more mass than spray material released from upwind nozzles (drop deposits were not recovered in either field study). The present report has addressed this subject in the following way:

1. We first re-examined the anemometer tower data to extract separate upwind and downwind vortex decay rates.

2. We then modified FSCBG to predict the McCooeye et al. (1993) data set, realizing that the Huddleston et al. (1994) paper did not contain enough information to study their results.

3. We found that FSCBG predicts the same upwind-downwind trends suggested by McCooeye et al. (1993) and Huddleston et al. (1994) for mass deposit. Data on number of drops were not recovered in either field study, although FSCBG number density predictions give a trend opposite that of mass deposit.

4. However, Young (1993) and Mickle (1993) raised important issues regarding the accuracy of the atomizations generated from the upwind and downwind nozzles (spray material from the upwind and downwind nozzles atomized differently in the wind tunnel, although a high obscuration was apparent).

5. This possible discrepancy suggests that the field study be repeated, with an eye toward quantifying the atomization accurately, and possibly alternating which side of the aircraft is upwind/downwind (one side was consistently maintained as "downwind" by McCooeye et al. 1993).

6. We then also realized that if very accurate data were recovered, the vortex model in FSCBG would probably have to be improved to enable the model to predict accordingly. Stability effects would require a model improvement as well.

# 8. CONCLUSIONS

A re-examination of available tower anemometer data has shown that upwind and downwind wingtip vortex strengths decay at different rates in a crosswind. When these decay rates are programmed into the near-wake model in FSCBG, predictions consistent with the field data of McCooeye et al. (1993) and Huddleston et al. (1994) result. However, how much of the difference between deposit from upwind nozzles and deposit from downwind nozzles is due to different decay rates of the upwind and downwind vortices in crosswind, or to the possible differences in nozzle atomization, remains to be resolved.

Under the conditions tested (and probably in other cases as well -- but not in all cases), spray material released from downwind nozzles appears to drift more than spray material released from upwind nozzles, on a mass basis, but the opposite appears true for number of drops. The strength of the upwind vortex tends to capture the smaller drops and carry them farther downwind, while depositing more of the larger drops closer to the aircraft flight line than the downwind vortex would.

# 9. REFERENCES


Barry, J. W. 1989. Management Overview Program WIND. Proceedings of the 19th Conference on Agricultural and Forest Meteorology. American Meteorological Society. Charleston, SC. 160-162.

Bilanin, A. J., M. E. Teske, J. W. Barry and R. B. Ekblad. 1989a. Project WIND Anemometer Tower Flyby Data Reduction. Proceedings of the 19th Conference on Agricultural and Forest Meteorology. American Meteorological Society: Charleston, SC. 188-201.

Bilanin, A. J., M. E. Teske, J. W. Barry and R. B. Ekblad. 1989b. AGDISP: The Aircraft Spray Dispersion Model, Code Development and Experimental Validation. *Transactions of the American Society of Agricultural Engineers* 32(1): 327-334.

Bilanin, A. J., M. E. Teske and J. E. Hirsh. 1978. Neutral Atmospheric Effects on the Dissipation of Aircraft Vortex Wakes. *AIAA Journal* 16(9): 956-961.

Chua, K. and T. R. Quackenbush. 1992a. A Fast Three-Dimensional Vortex Method for Unsteady Wake Calculations. Paper No. AIAA-92-2624-CP. Presented at the 10th AIAA Applied Aerodynamics Conference: Palo Alto, CA.

Chua, K. and T. R. Quackenbush. 1992b. A Fast Vortex Method for the Simulation of Three-Dimensional Flows on Parallel Computers. Parallel Computational Fluid Dynamics (J. Hauser, ed). Elsevier Science Publishers B. V.: Amsterdam, The Netherlands.

Chua, K., A. H. Boschitsch, P. Koumoutsakos, G. Winckelmans and A. Leonard. 1994. Numerical Simulation of Chemically-Reacting Shear-Layers via Three-Dimensional Fast Particle Methods. Paper No. AIAA-94-0675. Presented at the 32nd Aerospace Sciences Meeting and Exhibit: Reno, NV.

Huddleston, E. W., J. B. Ross, T. M. Ledson, R. Sanderson, G. M. Kilgore and D. L. Clason. 1994. Right Wind - Left Wing Difference in Drift. Paper No. AA94-004. Presented at the 1994 NAAA/ASAE Joint Technical Session: Las Vegas, NV.

McCooeye, M. A., R. S. Crabbe, R. E. Mickle, A. Robinson, E. B. Stimson, J. A. Arnold and D. G. Alward. 1993. Strategy for Reducing Drift of Aerially Applied Pesticides. National Research Council Canada Institute for Environmental Chemistry.

Mickle, R. E. 1993. Comments on the Vortex Study in New Mexico. Memorandum to B. W. Young dated 16 November 1993.

Mickle, R. E. 1995. Private Communication.

Teske, M. E. 1986. Field Study of Interaction of Spray Aircraft Wake with Convective Surface Winds in Hilly Terrain. Report No. 86-05. Continuum Dynamics, Inc.: Princeton, NJ.

Teske, M. E. 1988. AGDISP Analysis of Vortex Decay from Program WIND Phases I and III. Technical Note No. 88-06. Continuum Dynamics, Inc.: Princeton, NJ.

Teske, M. E., A. J. Bilanin and J. W. Barry. 1993. Decay of Aircraft Vortices Near the Ground. *AIAA Journal* 31(8): 1531-1533.

Teske, M. E., J. F. Bowers, J. E. Rafferty and J. W. Barry. 1993. FSCBG: An Aerial Spray Dispersion Model for Predicting the Fate of Released Material Behind Aircraft. *Environmental Toxicology and Chemistry* 12(3): 453-464.

Teske, M. E., A. E. Kaufman and T. B. Curbishley. 1988. Dugway Tower Flyby Data Collection, Reduction and Interpretation. Technical Note No. 88-11. Continuum Dynamics, Inc.: Princeton, NJ.

Teske, M. E., A. E. Kaufman and T. B. Curbishley. 1990. Additional Dugway Tower Flyby Data Collection, Reduction and Interpretation. Technical Note No. 90-14. Continuum Dynamics, Inc.: Princeton, NJ.

Williamson, G. G., M. E. Teske and R. G. Geyer. 1985. Experimental Study of Aircraft Wakes in Forest Canopies. Report No. 85-07. Continuum Dynamics, Inc.: Princeton, NJ.

Winckelmans, G. S. and A. Leonard. 1993. Contributions to Vortex Particle Methods for the Computation of Three-Dimensional Incompressible Unsteady Flows. *Journal of Computational Physics* 109(2): 247-273.

Young, B. W. 1993. Correspondence to M. A. McCooeye dated 15 November 1993.